Astronomical and Astrophysical Transactions (*AApTr*), 2026, Vol. 36, Issue 1, pp. 37–50,
ISSN 1055-6796, Photocopying permitted by license only, ©Cambridge Scientific Publishers

The Cepheid V415 Cen: variability type and pulsation stability

L.N. Berdnikov[1,*], S.V. Ivanova[2]

[1] *Sternberg Astronomical Institute, Moscow State University, Universitetskii pr. 13, Moscow, 119992 Russia*
[2] *Physical Faculty, Moscow State University, Universitetskij pr. 13, Moscow 119992, Russia*

Received 31 January, 2026; accepted 4 February, 2026

For the RV Tau-type star V415 Cen, we created an $O-C$ diagram spanning 135 years. This allowed us to calculate the rate of evolutionary period decrease for the first time: $dP/dt = -104.1\ (\pm 4.4)$ s yr^{-1}. Lombard and Koen's stability test confirmed the reality of this period decrease. If this decrease is indeed evolutionary, the final crossing of the instability strip before reaching the white dwarf cooling sequence seems a plausible explanation for V415 Cen's evolutionary status. As an RV Tau star, V415 Cen is likely a post-asymptotic giant branch star.

Keywords: Stars: variables: type II cepheids; stars: oscillations; stars: evolution

1 Introduction

Hoffleit (1936) discovered variable star HV7380 on photographic plates from Harvard University, and McLeod and Swope (1941) determined its period to be $26.^d735$. In the General Catalogue of Variable Stars (GCVS, Samus et al., 2017), it is listed as a CWA Cepheid with a period of $26.^d6523$. However, in Gaia Data Release 2 (Gaia DR2), it was classified as a T2CEP with a slightly different period of $26.^d656$ (Clementini et al., 2019), and later reclassified as a classical Cepheid with a period of $26.^d68846$ (Ripepi et al., 2019). In SIMBAD, V415 Cen is listed as an RVTAU variable star.

The purpose of this work is to clarify the type of V415 Cen variability and to investigate the stability of its pulsation period.

2 Light curves of V415 Cen

Figure 1 presents the light curves of V415 Cen, derived from ASAS-SN observations (Jayasinghe et al., 2019). The curves are displayed across three different JD intervals:

*Email: lberdnikov@gmail.com

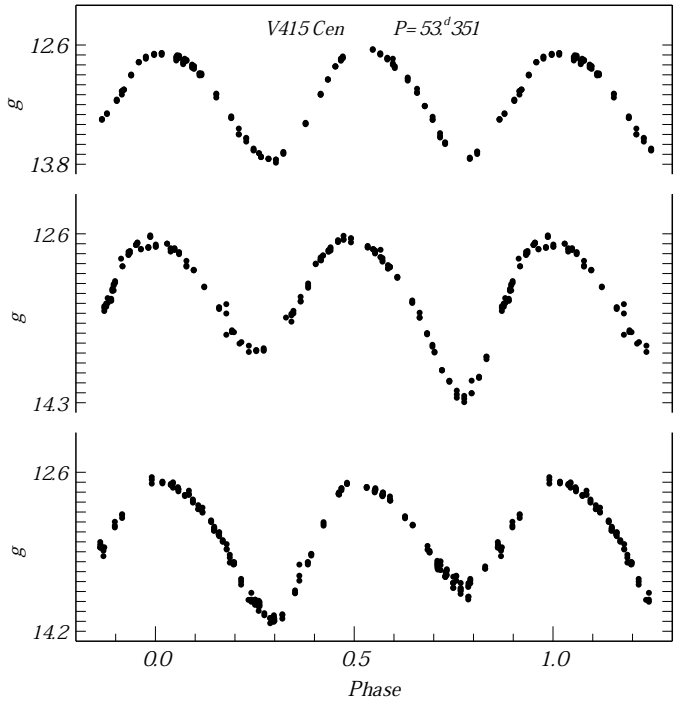


Figure 1 Light curves of V415 Cen in three JD intervals (from top to bottom): 2458476–2458530, 2458680–2458742, and 2459700–2459800.

2458476–2458530 at the top, 2458680–2458742 in the middle, and 2459700–2459800 at the bottom.

These light curves clearly indicate that V415 Cen is an RV Tau variable (RVA type according GCVS) with a period of $53.^d351$.

3 Variability of the period of V415 Cen

To investigate the behavior of the period of V415 Cen, we employ the standard approach of examining the $O-C$ diagram. The most precise method for calculating the $O-C$ residuals is the method developed by Hertzsprung (1919), whose computer implementation was described by Berdnikov (1992). To validate the observed period variations, we utilize the method proposed by Lombard and Koen (1993).

This study utilized data from various ground-based and space-based CCD surveys, including ASAS-3 (Pojmanski, 2002), ASAS-SN (Kochanek et al., 2017; Jayasinghe et al. 2019), and the Catalina Sky Survey (Drake et al., 2013). Additionally, we used photographic data from the DASCH project (Grindlay et al., 2012) and photoelectric data which were taken from the paper by Berdnikov et al. (2023).

Information on the number of observations used is given in Table 1.

Table 1 Observational data for V415 Cen.

Data source	Number of observations	Band of observations	JD interval
DASCH	825	Photographic, *pg*	2411510–2447773
Literature	31	Photoelectric, *BV*	2455906–2455950
ASAS	799	CCD, *V*	2451900–2455088
ASAS-SN	5683	CCD, *Vg*	2456792–2460936
CATALINA	161	CCD, *V*	2453611–2456419

The oldest photographic plate with the V415 Cen image was obtained at Harvard University in 1890, and the last CCD observations were made in 2025. Therefore, our data cover a time interval of 135 years.

4 Results and discussion

The results of processing seasonal V415 Cen curves are shown in Table 2. The first and second columns show the moments of maximum brightness and the errors in their determination, the third column shows the type of observations used, the fourth and fifth columns show the epoch number E and the $O-C$ residual, and the sixth and seventh columns show the number of observations N and the data source.

Data from Table 2 are shown in the $O-C$ diagram (Fig. 2) as dots with the error bars. Figure 2 shows frequent and abrupt period jumps, especially for $JD > 2450000$.

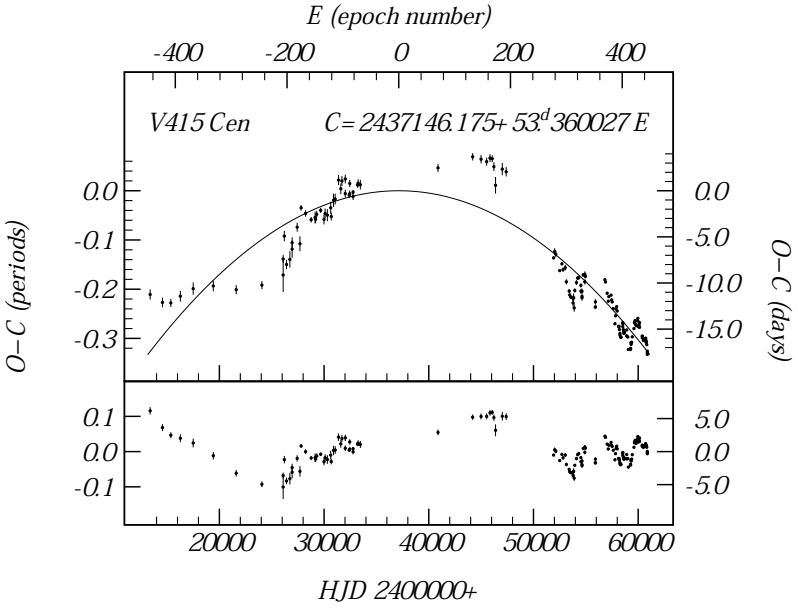


Figure 2 $O-C$ diagram for V415 Cen relative to the linear (top) and quadratic (bottom) elements (1). The line is a parabola corresponding to the light elements (1).

This part of the $O-C$ diagram is depicted in Fig. 3, which, due to the abundance of observations, allows us to discern even the most minute details. For photographic data, a calculation of the $O-C$ residuals from a small number of observations on long time intervals leads to larger errors as well as to a smoothing of the $O-C$ graph.

Table 2 Times of maximum light of V415 Cen.

Max, HJD	Uncertainty (days)	Filter	E	$O-C$ (days)	N	Data source
2413387.8756	0.5598	*pg*	−445	−13.0875	18	DASCH
2414560.9350	0.5230	*pg*	−423	−13.9487	20	DASCH
2415361.2797	0.4437	*pg*	−408	−14.0044	20	DASCH
2416269.1317	0.5922	*pg*	−391	−13.2729	20	DASCH
2417497.2336	0.6648	*pg*	−368	−12.4517	21	DASCH
2419418.4844	0.5718	*pg*	−332	−12.1618	21	DASCH
2421605.8399	0.4953	*pg*	−291	−12.5674	21	DASCH
2424060.8968	0.4338	*pg*	−245	−12.0718	19	DASCH
2426089.6744	1.8343	*pg*	−207	−10.9752	20	DASCH
2426091.4146	0.4437	*pg*	−207	−9.2350	21	DASCH
2426200.6137	0.5644	*pg*	−205	−6.7559	17	DASCH
2426410.9758	0.5117	*pg*	−201	−9.8340	19	DASCH
2426731.6841	0.8908	*pg*	−195	−9.2858	33	DASCH
2426946.2379	0.9236	*pg*	−191	−8.1721	24	DASCH
2426946.9432	0.5769	*pg*	−191	−7.4668	19	DASCH
2427428.8641	0.4808	*pg*	−182	−5.7861	20	DASCH
2427693.8639	0.8080	*pg*	−177	−7.5865	25	DASCH
2427804.4812	0.2977	*pg*	−175	−3.6892	21	DASCH
2428230.7531	0.3557	*pg*	−167	−4.2976	20	DASCH
2428763.6741	0.3020	*pg*	−157	−4.9769	20	DASCH
2429137.4252	0.6563	*pg*	−150	−4.7459	27	DASCH
2429190.5940	0.4034	*pg*	−149	−4.9372	30	DASCH
2429297.8565	0.3695	*pg*	−147	−4.3947	21	DASCH
2429671.8063	0.2709	*pg*	−140	−3.9651	20	DASCH
2429990.9792	0.5344	*pg*	−134	−4.9524	20	DASCH
2430098.3523	0.5314	*pg*	−132	−4.2993	31	DASCH
2430311.6084	0.6568	*pg*	−128	−4.4833	20	DASCH
2430632.5701	0.6573	*pg*	−122	−3.6818	24	DASCH
2430684.9783	0.4283	*pg*	−121	−4.6336	21	DASCH
2430900.1865	0.7170	*pg*	−117	−2.8655	29	DASCH
2431060.3936	0.5815	*pg*	−114	−2.7385	21	DASCH
2431382.6105	0.5590	*pg*	−108	−0.6817	21	DASCH
2431595.1077	0.5851	*pg*	−104	−1.6246	30	DASCH
2431702.6724	0.5314	*pg*	−102	−0.7801	21	DASCH
2432021.4647	0.4289	*pg*	−96	−2.1478	20	DASCH
2432023.0501	0.4807	*pg*	−96	−0.5625	30	DASCH
2432394.8265	0.2959	*pg*	−89	−2.3062	21	DASCH
2432448.3223	0.3669	*pg*	−88	−2.1705	29	DASCH

Table 2 (continued)

Max, HJD	Uncertainty (days)	Filter	E	$O-C$ (days)	N	Data source
2432449.4408	0.3994	*pg*	−88	−1.0520	27	DASCH
2432768.1901	0.3801	*pg*	−82	−2.4628	27	DASCH
2432768.6600	0.2531	*pg*	−82	−1.9929	21	DASCH
2433196.3336	0.2902	*pg*	−74	−1.1996	20	DASCH
2433249.8738	0.4329	*pg*	−73	−1.0194	29	DASCH
2433463.1508	0.5295	*pg*	−69	−1.1825	20	DASCH
2440882.0184	0.4415	*pg*	70	0.6413	16	DASCH
2444191.5425	0.4039	*pg*	132	1.8438	23	DASCH
2444991.6826	0.4605	*pg*	147	1.5834	21	DASCH
2445525.0209	0.4381	*pg*	157	1.3215	21	DASCH
2445845.5595	0.4326	*pg*	163	1.6999	21	DASCH
2446058.9421	0.3623	*pg*	167	1.6423	21	DASCH
2446218.1496	0.4727	*pg*	170	0.7698	21	DASCH
2446376.2113	0.9035	*pg*	173	−1.2486	20	DASCH
2447018.2856	0.6721	*pg*	185	0.5054	19	DASCH
2447391.5231	0.5093	*pg*	192	0.2227	22	DASCH
2451919.6282	0.1569	*V*	277	−7.2744	20	ASAS-3
2452027.0494	0.3489	*V*	279	−6.5733	22	ASAS-3
2452133.4590	0.3311	*V*	281	−6.8838	20	ASAS-3
2452505.2047	0.1399	*V*	288	−8.6583	19	ASAS-3
2452719.3814	0.1587	*V*	292	−7.9217	42	ASAS-3
2452825.4705	0.2411	*V*	294	−8.5527	42	ASAS-3
2453039.1267	0.3076	*V*	298	−8.3366	27	ASAS-3
2453144.3137	0.2806	*V*	300	−9.8696	27	ASAS-3
2453410.1058	0.2236	*V*	305	−10.8777	25	ASAS-3
2453463.0455	0.2205	*V*	306	−11.2980	35	ASAS-3
2453569.5241	0.2165	*V*	308	−11.5394	33	ASAS-3
2453782.3401	0.3889	*V*	312	−12.1635	26	ASAS-3
2453782.8322	0.3225	*V*	312	−11.6714	20	ASAS-3
2453836.2742	0.4494	*V*	313	−11.5895	19	ASAS-3
2453888.5248	0.4141	*V*	314	−12.6989	25	ASAS-3
2453943.7720	0.2215	*V*	315	−10.8117	53	CATALINA
2454104.7108	0.2547	*V*	318	−9.9530	38	ASAS-3
2454211.9179	0.2224	*V*	320	−9.4660	39	ASAS-3
2454318.6738	0.2155	*V*	322	−9.4301	38	ASAS-3
2454530.6598	0.2675	*V*	326	−10.8842	34	ASAS-3
2454531.2799	0.2234	*V*	326	−10.2641	29	ASAS-3
2454636.6566	0.3079	*V*	328	−11.6075	30	ASAS-3
2454636.8187	0.2368	*V*	328	−11.4454	32	ASAS-3
2454637.3611	0.2896	*V*	328	−10.9030	36	ASAS-3
2454745.8616	0.1864	*V*	330	−9.1225	53	CATALINA
2454905.1899	0.2905	*V*	333	−9.8743	32	ASAS-3
2454906.0045	0.3195	*V*	333	−9.0597	27	ASAS-3

Table 2 (continued)

Max, HJD	Uncertainty (days)	Filter	E	$O-C$ (days)	N	Data source
2454959.1393	0.2279	V	334	−9.2849	42	ASAS-3
2455914.4625	0.1195	B	352	−12.6045	31	Berdnikov et al. (2023)
2455916.3002	0.1039	V	352	−12.6045	31	Berdnikov et al. (2023)
2455916.8542	0.3032	V	352	−12.0505	55	CATALINA
2456826.3772	0.1072	V	369	−9.6479	49	ASAS-SN
2456879.4923	0.0937	V	370	−9.8929	49	ASAS-SN
2457038.3541	0.1505	V	373	−11.1112	62	ASAS-SN
2457144.2069	0.1176	V	375	−11.9784	58	ASAS-SN
2457198.0717	0.0756	V	376	−11.4737	57	ASAS-SN
2457411.6644	0.0636	V	380	−11.3210	53	ASAS-SN
2457464.5097	0.1444	V	381	−11.8358	54	ASAS-SN
2457517.6506	0.1130	V	382	−12.0550	58	ASAS-SN
2457623.6528	0.0828	V	384	−12.7728	80	ASAS-SN
2457782.0876	0.1259	V	387	−14.4181	76	ASAS-SN
2457836.3093	0.1470	V	388	−13.5564	64	ASAS-SN
2457890.3837	0.0710	V	389	−12.8421	60	ASAS-SN
2457944.0220	0.0710	V	390	−12.5637	50	ASAS-SN
2457996.9112	0.1311	V	391	−13.0346	50	ASAS-SN
2458154.1176	0.0877	g	394	−14.7263	80	ASAS-SN
2458154.1440	0.0613	g	394	−14.6999	130	ASAS-SN
2458155.3126	0.0495	V	394	−14.7133	100	ASAS-SN
2458208.3352	0.1511	V	395	−15.0507	60	ASAS-SN
2458259.9119	0.1209	g	396	−15.6521	81	ASAS-SN
2458260.0974	0.1414	g	396	−15.4666	80	ASAS-SN
2458314.2485	0.0728	V	397	−15.8575	81	ASAS-SN
2458366.3979	0.0743	g	398	−15.8862	75	ASAS-SN
2458527.6373	0.0572	g	401	−14.7268	89	ASAS-SN
2458527.9472	0.0539	g	401	−14.4169	87	ASAS-SN
2458528.0762	0.0611	g	401	−14.2879	75	ASAS-SN
2458580.6744	0.0505	g	402	−15.0497	100	ASAS-SN
2458633.6228	0.0576	g	403	−15.4613	100	ASAS-SN
2458633.8074	0.0659	g	403	−15.2767	93	ASAS-SN
2458687.0493	0.1214	g	404	−15.3949	96	ASAS-SN
2458687.0809	0.0698	g	404	−15.3633	106	ASAS-SN
2458900.1405	0.2103	g	408	−15.7438	50	ASAS-SN
2458900.7976	0.0951	g	408	−15.0867	64	ASAS-SN
2459006.7503	0.1260	g	410	−15.8540	104	ASAS-SN
2459058.7547	0.1024	g	411	−17.2097	49	ASAS-SN
2459272.1974	0.0809	g	415	−17.2071	80	ASAS-SN
2459272.3270	0.0705	g	415	−17.0775	80	ASAS-SN
2459326.1128	0.0640	g	416	−16.6517	75	ASAS-SN

Table 2 (continued)

Max, HJD	Uncertainty (days)	Filter	E	$O-C$ (days)	N	Data source
2459326.2681	0.0790	g	416	−16.4964	135	ASAS-SN
2459326.3200	0.0654	g	416	−16.4445	70	ASAS-SN
2459379.6891	0.0637	g	417	−16.4355	83	ASAS-SN
2459433.6465	0.0966	g	418	−15.8381	83	ASAS-SN
2459594.6252	0.0934	g	421	−14.9395	102	ASAS-SN
2459648.5870	0.0480	g	422	−14.3377	100	ASAS-SN
2459648.6664	0.0657	g	422	−14.2583	102	ASAS-SN
2459702.2079	0.0985	g	423	−14.0768	89	ASAS-SN
2459755.1625	0.0994	g	424	−14.4822	101	ASAS-SN
2459755.5447	0.1372	g	424	−14.1000	104	ASAS-SN
2459808.3752	0.1119	g	425	−14.6296	94	ASAS-SN
2459968.9627	0.0792	g	428	−14.1221	104	ASAS-SN
2459969.2459	0.0651	g	428	−13.8390	82	ASAS-SN
2460021.7080	0.1037	g	429	−14.7369	95	ASAS-SN
2460075.1595	0.0468	g	430	−14.6454	105	ASAS-SN
2460075.3100	0.0988	g	430	−14.4949	113	ASAS-SN
2460128.3547	0.0679	g	431	−14.8103	99	ASAS-SN
2460128.8766	0.1104	g	431	−14.2883	77	ASAS-SN
2460394.0078	0.1029	g	436	−15.9572	97	ASAS-SN
2460394.1783	0.0477	g	436	−15.7867	92	ASAS-SN
2460394.2128	0.0875	g	436	−15.7523	124	ASAS-SN
2460500.4511	0.1177	g	438	−16.2340	90	ASAS-SN
2460500.6509	0.0730	g	438	−16.0342	100	ASAS-SN
2460713.9901	0.0595	g	442	−16.1351	90	ASAS-SN
2460714.1442	0.0495	g	442	−15.9810	69	ASAS-SN
2460767.0438	0.0650	g	443	−16.4415	80	ASAS-SN
2460767.1017	0.0711	g	443	−16.3836	74	ASAS-SN
2460767.1702	0.0337	g	443	−16.3150	100	ASAS-SN
2460820.1624	0.0570	g	444	−16.6829	70	ASAS-SN
2460872.4658	0.1270	g	445	−17.7395	63	ASAS-SN
2460872.6447	0.1811	g	445	−17.5606	62	ASAS-SN
2460872.8137	0.1083	g	445	−17.3916	81	ASAS-SN

The maximum brightness for pulsating stars is known to occur later as the effective wavelength of the photometric band increases. Therefore, when using data from different bands, we should choose the primary band (in this case, V) and determine the shifts in the time of maximum light in other bands based on simultaneous observations.

Based on the data in Table 2, we found that the maxima in the B and g bands occurred earlier than those in the V band by $1.^d8356$ and $1.^d1819$, respectively. We applied these corrections when calculating the $O-C$ residuals in Table 2, constructing Figs 2–5, and determining the light elements (1), which, thus, refer to the V band.

$$Max\ HJD = 2437146.175\ (\pm 0.352) + 53.360027\ (\pm 0.9560\ 10^{-3}) \cdot E - 0.87994873\ 10^{-4}\ (\pm 0.3743\ 10^{-5}) \cdot E^2. \quad (1)$$

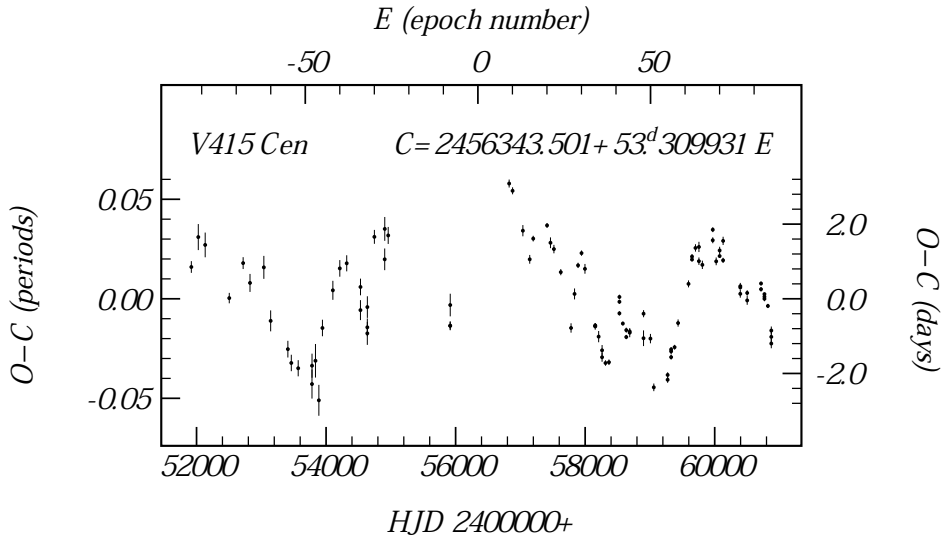


Figure 3 $O - C$ diagram for V415 Cen for $JD > 2450000$.

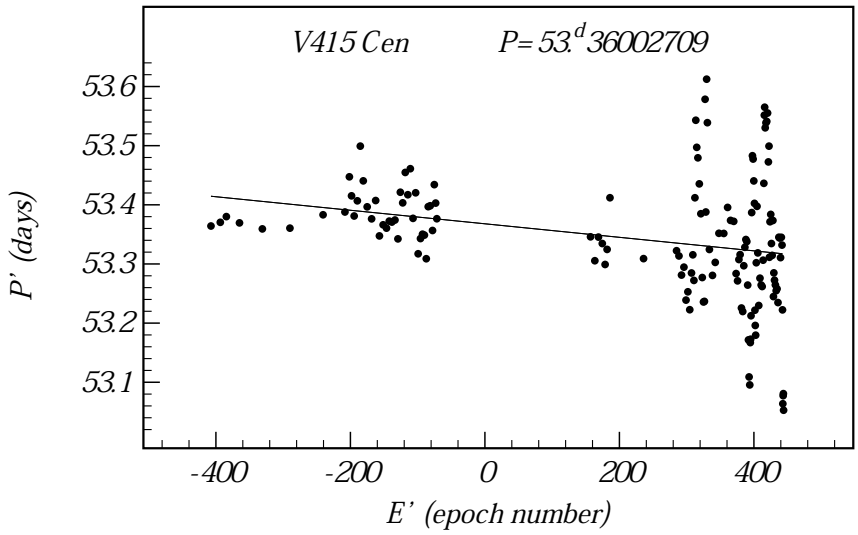


Figure 4 Dependence of $P'_i = P + [(O - C)_{i+1} - (O - C)_i)]/(E_{i+1} - E_i)$ on $E'_i = (E_i + E_{i+1})/2$. The line corresponds to the behavior of $O - C$ residuals in Fig. 3.

These quadratic elements make it possible to calculate the rate of secular decrease in the period, $dP/dt = -104.1$ (± 4.4) s yr^{-1}.

To confirm that the decrease in the pulsation period is real, we use the method published by Lombard and Koen (1993). For this purpose, we calculated the differences $\Delta(O - C)_i$ of the successive $O - C$ residuals from Table 2, $\Delta(O - C)_i = (O - C)_{i+1} - (O - C)_i$, and plotted $P'_i = P + [\Delta(O - C)_i/(E_{i+1} - E_i)]$ against

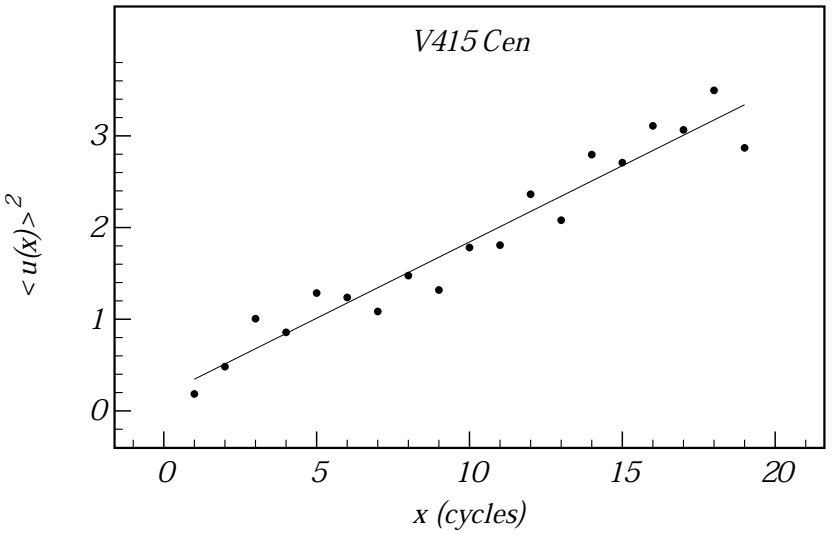


Figure 5 Dependence of the normalized scattering parameter Square of the mean accumulated delay $< u(x) >$ versus cycle difference x for V415 Cen. The line is the fit of Eq. (2) for $x < 20$, which gives the amplitude of random period fluctuations, $\varepsilon = 0.^d409 \pm 0.^d101$ ($\varepsilon/P \approx 0.008$).

$E'_i = (E_i + E_{i+1})/2$ (Fig. 4). The value of P'_i, which has the meaning of the average period in an epoch interval $E_{i+1} - E_i$, correspondis to the behavior of the $O - C$ residuals in Fig. 3.

If the decrease in the period is truly evolutionary, then the final crossing the instability strip before approaching the white dwarf cooling sequence seems to be a plausible explanation for the evolutionary status of V415 Cen, which as an RV Tau star, is most likely a post-asymptotic giant branch star (Bono et al., 2024).

The data in Table 2 allow to estimate the random fluctuations in the pulsation period. For this purpose, we calculated the delays $u(x) =\mid z_{x+i} - z_x \mid$ for the maxima z separated by x cycles. According to Eddington and Plakidis (1929), the mean $< u(x) >$ must be related to the random period fluctuation ε by the relation

$$< u(x) >^2 = 2\alpha^2 + x\varepsilon^2, \qquad (2)$$

where α characterizes the random errors in the measured times of maximum light.

As we noted above, the use of photographic observations leads to a smoothing of the $O - C$ graph, therefore, to calculate ε, we use only the data shown in Fig. 3. The results of our calculations are presented in Fig. 5 and point to the existence of a linear trend in in $< u(x) >^2$ for $x < 20$, where a formal fitting of Eq. (2) gives a solution in the form

$$< u(x) >^2 = 0.1726(\pm 0.1166) + 0.1668(\pm 0.0102)x,$$

whence the random period fluctuation is $\varepsilon = 0.^d409 \pm 0.^d101$. Thus, our data provide evidence for the existence of rather large random period fluctuations, which, nevertheless, do not mask the secular changes in the period.

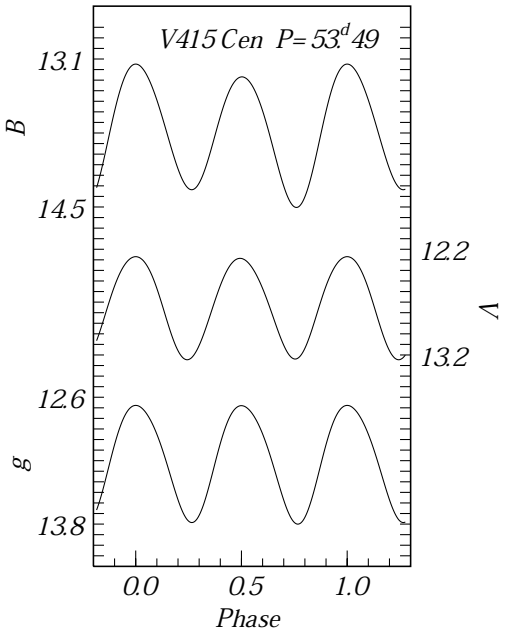


Figure 6 Standard light curves for V415 Cen in filters B, V, and g.

Note that the results obtained here are based on specific standard light curves. Therefore, we give them in Table 3 to be used in future studies and to establish a relationship to our data if other standard light curves are used. Table 3 contains the magnitudes of V415 Cen for phases from 0 to 0.995 in 0.005 increments in filters B, V, and g; these standard curves are graphically shown in Fig. 6.

The standard curve for filter B was created based on individual light curve (Berdnikov et al., 2023), while for filters V and g, we employed mean light curves derived from ASAS-SN data over a broad timeframe. This is the reason for the difference in the light curves in Figs 1 and 6.

Strictly speaking, the Hertzsprung method is applicable for variable stars with stable light curves, that is, the shape of the standard and observed light curves should be identical. In the case of V415 Cen, the changes in the light curve are insignificant, so the Hertzsprung method provides reliable data for studying the variability of its period.

Table 3 B-, V- and g-band standard curves of V415 Cen.

Phase	B	V	g	Phase	B	V	g	Phase	B	V	g
0.000	13.148	12.270	12.677	0.335	14.099	12.926	13.525	0.670	14.096	12.955	13.379
0.005	13.149	12.271	12.678	0.340	14.068	12.896	13.490	0.675	14.133	12.983	13.413
0.010	13.152	12.273	12.680	0.345	14.035	12.866	13.454	0.680	14.169	13.010	13.446
0.015	13.157	12.276	12.684	0.350	14.001	12.836	13.417	0.685	14.204	13.036	13.479
0.020	13.164	12.282	12.690	0.355	13.966	12.805	13.379	0.690	14.238	13.061	13.512
0.025	13.173	12.288	12.696	0.360	13.931	12.775	13.341	0.695	14.271	13.085	13.543
0.030	13.184	12.297	12.705	0.365	13.895	12.745	13.302	0.700	14.303	13.108	13.574
0.035	13.196	12.306	12.715	0.370	13.859	12.714	13.263	0.705	14.333	13.129	13.603
0.040	13.210	12.318	12.726	0.375	13.822	12.684	13.224	0.710	14.360	13.149	13.631
0.045	13.226	12.330	12.738	0.380	13.786	12.655	13.186	0.715	14.386	13.167	13.657
0.050	13.243	12.345	12.751	0.385	13.750	12.626	13.147	0.720	14.410	13.184	13.682
0.055	13.262	12.361	12.766	0.390	13.715	12.598	13.110	0.725	14.432	13.198	13.705
0.060	13.283	12.378	12.782	0.395	13.680	12.571	13.073	0.730	14.450	13.211	13.725
0.065	13.304	12.397	12.799	0.400	13.646	12.544	13.038	0.735	14.467	13.221	13.744
0.070	13.327	12.418	12.817	0.405	13.612	12.519	13.003	0.740	14.480	13.229	13.760
0.075	13.351	12.440	12.837	0.410	13.580	12.494	12.970	0.745	14.491	13.234	13.773
0.080	13.376	12.464	12.857	0.415	13.549	12.470	12.939	0.750	14.499	13.238	13.784
0.085	13.403	12.488	12.879	0.420	13.519	12.448	12.909	0.755	14.503	13.238	13.793
0.090	13.430	12.515	12.901	0.425	13.490	12.427	12.880	0.760	14.505	13.237	13.798
0.095	13.459	12.542	12.925	0.430	13.463	12.407	12.854	0.765	14.503	13.233	13.800
0.100	13.488	12.571	12.950	0.435	13.438	12.389	12.829	0.770	14.498	13.226	13.800
0.105	13.519	12.600	12.976	0.440	13.414	12.372	12.806	0.775	14.490	13.217	13.797
0.110	13.550	12.630	13.002	0.445	13.392	12.357	12.785	0.780	14.479	13.205	13.790
0.115	13.581	12.662	13.030	0.450	13.371	12.343	12.766	0.785	14.465	13.192	13.781
0.120	13.614	12.694	13.059	0.455	13.353	12.330	12.749	0.790	14.447	13.175	13.769
0.125	13.647	12.726	13.089	0.460	13.336	12.319	12.734	0.795	14.427	13.157	13.754
0.130	13.681	12.759	13.119	0.465	13.321	12.310	12.721	0.800	14.404	13.137	13.736

©2026 Astronomical and Astrophysical Transactions (AApTr), Vol. 36, Issue 1

Table 3 (continued)

Phase	B	V	g	Phase	B	V	g	Phase	B	V	g
0.135	13.714	12.792	13.150	0.470	13.308	12.302	12.709	0.805	14.378	13.115	13.715
0.140	13.749	12.825	13.182	0.475	13.297	12.296	12.700	0.810	14.349	13.091	13.692
0.145	13.783	12.857	13.214	0.480	13.287	12.291	12.692	0.815	14.318	13.065	13.667
0.150	13.818	12.890	13.247	0.485	13.280	12.288	12.686	0.820	14.284	13.038	13.639
0.155	13.852	12.922	13.280	0.490	13.274	12.286	12.682	0.825	14.248	13.010	13.609
0.160	13.886	12.953	13.313	0.495	13.271	12.286	12.680	0.830	14.210	12.980	13.577
0.165	13.920	12.983	13.347	0.500	13.269	12.287	12.679	0.835	14.170	12.950	13.544
0.170	13.954	13.013	13.380	0.505	13.269	12.290	12.680	0.840	14.129	12.919	13.509
0.175	13.987	13.041	13.413	0.510	13.271	12.294	12.683	0.845	14.087	12.887	13.472
0.180	14.019	13.068	13.446	0.515	13.275	12.299	12.687	0.850	14.043	12.855	13.435
0.185	14.051	13.093	13.478	0.520	13.280	12.306	12.692	0.855	13.998	12.823	13.396
0.190	14.082	13.117	13.510	0.525	13.288	12.314	12.699	0.860	13.953	12.790	13.358
0.195	14.111	13.139	13.541	0.530	13.297	12.323	12.707	0.865	13.907	12.758	13.318
0.200	14.140	13.160	13.570	0.535	13.307	12.334	12.716	0.870	13.861	12.726	13.278
0.205	14.167	13.178	13.599	0.540	13.320	12.346	12.727	0.875	13.815	12.694	13.239
0.210	14.192	13.194	13.626	0.545	13.334	12.359	12.739	0.880	13.769	12.663	13.199
0.215	14.216	13.208	13.651	0.550	13.350	12.373	12.752	0.885	13.724	12.633	13.160
0.220	14.238	13.220	13.675	0.555	13.367	12.388	12.767	0.890	13.680	12.604	13.122
0.225	14.258	13.230	13.697	0.560	13.386	12.405	12.782	0.895	13.636	12.575	13.085
0.230	14.276	13.237	13.717	0.565	13.406	12.422	12.799	0.900	13.594	12.548	13.048
0.235	14.292	13.242	13.734	0.570	13.429	12.441	12.817	0.905	13.552	12.521	13.013
0.240	14.305	13.245	13.749	0.575	13.452	12.460	12.836	0.910	13.512	12.496	12.979
0.245	14.317	13.245	13.762	0.580	13.477	12.480	12.856	0.915	13.474	12.472	12.946
0.250	14.325	13.243	13.772	0.585	13.503	12.502	12.877	0.920	13.438	12.449	12.916
0.255	14.332	13.239	13.779	0.590	13.531	12.524	12.899	0.925	13.403	12.427	12.886
0.260	14.336	13.233	13.784	0.595	13.560	12.547	12.923	0.930	13.370	12.407	12.859
0.265	14.337	13.224	13.786	0.600	13.590	12.571	12.947	0.935	13.340	12.389	12.833
0.270	14.335	13.214	13.784	0.605	13.622	12.595	12.973	0.940	13.311	12.371	12.809

©2026 Astronomical and Astrophysical Transactions (AApTr), Vol. 36, Issue 1

Table 3 (continued)

Phase	B	V	g	Phase	B	V	g	Phase	B	V	g
0.275	14.332	13.201	13.780	0.610	13.654	12.620	12.999	0.945	13.285	12.355	12.788
0.280	14.325	13.186	13.773	0.615	13.688	12.646	13.027	0.950	13.261	12.340	12.768
0.285	14.316	13.170	13.764	0.620	13.722	12.673	13.056	0.955	13.239	12.327	12.750
0.290	14.304	13.151	13.751	0.625	13.758	12.700	13.085	0.960	13.219	12.315	12.734
0.295	14.290	13.131	13.735	0.630	13.794	12.728	13.116	0.965	13.203	12.305	12.720
0.300	14.274	13.110	13.717	0.635	13.831	12.756	13.147	0.970	13.188	12.295	12.709
0.305	14.255	13.087	13.696	0.640	13.868	12.784	13.179	0.975	13.175	12.288	12.699
0.310	14.234	13.062	13.673	0.645	13.906	12.813	13.211	0.980	13.165	12.281	12.691
0.315	14.210	13.037	13.648	0.650	13.944	12.842	13.244	0.985	13.158	12.276	12.685
0.320	14.185	13.010	13.620	0.655	13.982	12.870	13.278	0.990	13.152	12.273	12.680
0.325	14.158	12.983	13.590	0.660	14.020	12.899	13.311	0.995	13.149	12.271	12.678
0.330	14.129	12.955	13.558	0.665	14.058	12.927	13.345				

Conclusions

To study the period variability of V415 Cen, which turned out to be an RV Tau type star, we collected 825 magnitude estimates on old photographic plates and 6674 published observations in filters B, V, and g. We processed all available data using the Hertzsprung method (1919) and constructed the $O-C$ diagram covering a time interval of 135 years. Our data indicate the presence of significant random fluctuations in the period, $\varepsilon = 0.^d409 \pm 0.^d101$. They do not mask the parabola in the $O-C$ diagram, which allows us to estimate the rate of secular decrease of the period, $dP/dt = -104.1$ (± 4.4) s yr^{-1}. The pulsation stability test proposed by Lombard and Koen (1993) confirmed that the period decrease is real. If this decrease is indeed evolutionary, the final crossing of the instability strip before reaching the white dwarf cooling sequence seems a plausible explanation for V415 Cen's evolutionary status.

Acknowledgments

The study was conducted under the state assignment of Lomonosov Moscow State University.

References

Berdnikov L.N. (1992) Sov. Astron. Lett. **18**, 207
Berdnikov L.N., Kniazev A.Yu., Dambis A.K., Kravtsov V.V. and Pastukhova E.N. (2023) Variable stars **43**, 86
Bono G., Braga V.F. and Pietrinferni A. (2024) Astron. Astrophys. Rev. **32**, 4.
Clementini G., Ripepi V., Molinaro R., Garofalo A., Muraveva T., et al. (2019) Astron. Astrophys. **622**, A60
Eddington A.S. and Plakidis) S. (1929) Mon. Not. R. Astron. Soc. **90**, 65
Grindlay J., Tang S., Simcoe R., Laycock S., Los E., et al. (2009) ASP Conf. Ser. **410**, 101
Hertzsprung E. (1919) Astron. Nachr **210**, 17
Hoffleit D. (1936) Harvard Bull. **902**, 13
Jayasinghe T., Stanek K.Z., Kochanek C.S., Shappee B.J., Holoien, T.W.-S. et al. (2019) Mon. Not. R. Astron. Soc. **485**, 961
Kochanek C.S., Shappee B.J., Stanek K.Z., Holoien T.W.S., Thompson Todd A., et al. (2017) Publ. Astron. Soc. Pac. **129**, 104502
Lombard F. and Koen C. (1993) Mon. Not. R. Astron. Soc. **263**, 309
McLeod N.W. and Swope H.H. (1941) Harvard Bull. **915**, 29
Pojmanski G. (2002) Acta Astron. **52**, 397
Ripepi V., Molinaro R., Musella I, Marconi M., Leccia S. and Eyer L. (2019) Astron. Astrophys. **625**, A14
Samus N.N., Kazarovets E.V., Durlevich O.V., Kireeva N.N. and Pastukhova E.N. (2017) Astron. Rep. **61**, 80